ELSEVIER

Polymer Vol. 37 No. 1, pp. 57–64, 1996

0032-3861/96/$15.00+0.00

Tensile properties of highly syndiotactic polypropylene

Hiroki Uehara, Yoshihiro Yamazaki and Tetsuo Kanamoto*
Department of Applied Chemistry, Science University of Tokyo, Kagurazaka, Shinjuku-ku, Tokyo 162, Japan
(Received 22 December 1994; revised 6 March 1995)

The tensile properties and uniaxial drawing of highly syndiotactic polypropylene (s-PP) have been studied. The results were compared to those of isotactic polypropylene (i-PP) having a comparable molecular weight, molecular-weight distribution and stereoregularity. S-PP and i-PP of different initial morphologies, prepared by crystallization from the melt and solution, were drawn by solid-state coextrusion and tensile drawing. The structure and properties of drawn films have been characterized by wide- and small-angle X-ray diffraction, stress–strain behaviour, etc. The maximum achievable draw ratio (*DR*) for s-PP was 5–10, depending on the initial morphologies, and significantly lower than that for i-PP ($DR \leq 30$). The poor ductility of s-PP was ascribed to the absence of a crystalline relaxation, which was clearly observed in the highly drawable i-PP by dynamic mechanical tests. The tensile properties of drawn films increased with *DR* for each of the PPs. At a given *DR*, however, the modulus was remarkably lower for s-PP than for i-PP, yet the tensile strengths were not significantly different. The maximum tensile modulus and strength of s-PP achieved in this work were 3.0 and 0.33 GPa, respectively. These values were remarkably lower than those (20 and 0.60 GPa, respectively) achieved for an i-PP having comparable molecular characteristics, reflecting the low crystal modulus, drawability and crystallinity of s-PP compared to those of i-PP. The structural change on drawing of s-PP was also discussed.

(Keywords: syndiotactic polypropylene; drawability; tensile properties)

INTRODUCTION

Recently, highly syndiotactic PP (s-PP) has become available by polymerization using Ewen's[1] catalyst system composed of isopropylidene(cyclopentadienyl)(9-fluorenyl)zirconium or hafnium dichloride and methylaluminoxane. The structure and properties of this polymer have received considerable attention. It has been shown that this polymer takes three crystal modifications: the most stable form I[2–4], and metastable form II[5, 6] and III[7]. The thermal properties of s-PP with low[8, 9] and high[10, 11] syndiotacticity have been reported. Previously, we[12] have also discussed the origin of d.s.c. double melting endotherms, the heat of fusion for a perfect crystal of the most stable form I, and the thermodynamic equilibrium melting temperature for a fully syndiotactic PP, using a series of high syndiotactic PP samples. The mechanical properties of s-PP are also important and interesting. Nevertheless, only a few reports[13, 14] have been published on these properties.

In a previous paper[15], we have shown that single-crystal mats of ultrahigh-molecular-weight i-PP (UHMW i-PP), precipitated from dilute solutions in xylene, could be effectively ultradrawn to draw ratios (*DR*) up to about 80. Such superdrawn films exhibited tensile moduli and strength of ≤ 37 and ≤ 2.0 GPa, respectively. The maximum modulus value approaches the theoretical crystal modulus of i-PP (35–42 GPa)[16, 17], indicating that an extreme chain extension and orientation were achieved by drawing from single-crystal mats. The purpose of this work is manifold: first, to study the drawing behaviour of highly syndiotactic PP having different initial morphologies; secondly, to determine the tensile and morphological properties of drawn products; thirdly, to compare these results to those of i-PP having comparable molecular weight, molecular-weight distribution and stereoregularity; and fourthly, to study the morphological change during drawing.

*To whom correspondence should be addressed

EXPERIMENTAL

Samples

The samples used in this work were two s-PPs (s-PP-1, s-PP-2) and an i-PP. For most of the experiments, s-PP-2 was used, unless otherwise noted. *Table 1* shows syndiotactic (*SPF*) and isotactic pentad fractions (*IPF*) determined by ^{13}C n.m.r, and weight- (M_w) and number-average molecular weights (M_n) and molecular-weight distribution (M_w/M_n) evaluated by g.p.c.

The conventional i-PP polymerized by using a Ziegler–Natta catalyst system has a M_w/M_n much larger than those ($M_w/M_n = 2$–3) of s-PP prepared by Ewen's catalyst system. To prepare an i-PP sample having a comparable M_w and M_w distribution, the higher-molecular-weight component of a high-M_w i-PP was selectively degraded by treating with t-butylcumylperoxide. UHMW i-PP having a M_w of

Table 1 Tacticities, molecular weights and molecular-weight distributions of s-PP and i-PP samples

	SPF^a	IPF^b	$10^4 M_w$	$10^4 M_w$	M_w/M_n
s-PP-1	0.945	–	20.2	11.2	1.8
s-PP-2	0.936	–	18.0	6.0	3.0
i-PP	–	0.934	23.6	10.4	2.3

[a] Syndiotactic pentad fraction evaluated by ^{13}C n.m.r.
[b] Isotactic pentad fraction evaluated by ^{13}C n.m.r.

2.4×10^6 was dissolved in hot xylene to prepare a 1 wt% solution. The solution was cooled to room temperature, and 40 wt% of the peroxide (based on polymer) was added to the solution. The mixture was slowly heated to the boiling point, and kept there for ~ 8 h to allow the reaction to be completed. After the reaction, the solution was poured into excess methanol. To degrade a small amount of the residual peroxide, the precipitate was heated at 165°C for 8 h *in vacuo*. The i.r. spectra measured before and after the peroxide treatments were identical, showing that chain scission was the predominant mechanism for the reaction. The treatment with peroxide was repeated on the product until the desired M_w and M_w/M_n were achieved.

Preparation of melt- and solution-crystallized samples

Melt-crystallized films of s-PP and i-PP were prepared by compression moulding at 200°C for each polymer containing a small amount of an antioxidant (2,6-di-t-butyl-*p*-cresol), followed by (1) slow cooling to room temperature (MSC) and (2) quenching at −70°C (MQ). The crystallinities of MSC and MQ samples, calculated from the densities, were 44 and 29% respectively, for s-PP, and 68 and 57%, respectively, for i-PP.

Solution-grown crystal (SGC) mats of s-PP were prepared as follows. A 0.2 wt% solution was prepared by dissolving an appropriate amount of s-PP in 400 ml of xylene, containing 0.1 wt% (based on solvent) of an antioxidant, at 110°C under a N_2 gas flow. The hot solution was cooled to room temperature to precipitate crystals. The crystal suspension was again heated slowly to 100°C, to obtain a homogeneous solution with stabilized nuclei, followed by isothermal crystallization at 45°C. A sedimented mat of s-PP SGC was obtained by slowly filtering the crystal suspension, followed by drying *in vacuo* at room temperature. The crystallinity of an SGC mat was 63%, as calculated from the density measured by a pycnometer using 2-propanol as a filling fluid.

Drawing

Three techniques were applied for drawing of s-PP and i-PP, i.e. solid-state coextrusion[18], conventional tensile drawing and two-stage drawing (their sequential combination)[19]. SGC mats of s-PP were brittle and draw was not attainable by a straight tensile drawing. MSC films of s-PP also showed poor ductility for tensile drawing at elevated temperatures. Thus, these two morphologies of s-PP were drawn by solid-state coextrusion. For this, a strip of 3 mm × 0.3 mm × 30 mm was placed between two longitudinally split billet halves of linear low-density polyethylene (LLDPE), high-density polyethylene (HDPE) or poly(4-methyl-1-pentane), and the assembly coextruded at 60–145°C through conical dies having nominal extrusion draw ratio (*EDR*) of 2–16.

MQ films of s-PP and both MSC and MQ films of i-PP could be effectively tensile drawn at elevated temperatures. These samples were drawn at constant temperatures of 60–145°C and at constant extension cross-head speeds in an air oven equipped with Orientec Tensilon tensile tester type RTM-100. For two-stage drawing, s-PP films were drawn first by solid-state coextrusion to an *EDR* of 3–6, followed by further tensile drawing at 100–145°C. The draw ratio (*DR*) was determined from the separation of ink marks preimprinted on the surface of samples.

Measurements

Transmission electron microscopic observations of solution-grown crystals of s-PP were made with a Hitachi type H-800 electron microscope operated at 100 kV. Wide-angle X-ray diffraction (WAXD) and small-angle X-ray scattering (SAXS) patterns were recorded on a Rigaku flat-plate camera and a JEOL type DX-LS-1 small-angle vacuum camera, respectively. Ni-filtered Cu Kα radiation used was generated by Rigaku-Denki X-ray generators RAD-III-A and RU-200.

Birefringence was measured by using an Olympus Berek compensator and an optical microscope model BHSP. Densities of drawn films were determined at 30°C in a density gradient column consisting of a mixture of 2-propanol and diethyleneglycol monomethyl ether. As the initial SGC mat contained voids, the density was measured at 30°C by a pycnometer using 2-propanol as a filling fluid. To remove the air trapped in the mat, a pycnometer containing pieces of mats and the liquid was kept under a reduced pressure of 40 mmHg for 3 h. Crystallinity was calculated from the densities, assuming a crystal/amorphous two-phase model. The densities of form I crystalline and amorphous s-PP were assumed to be 0.930 (refs. 2, 3) and 0.858 g cm^{-3} (refs 20, 21), respectively.

The tensile modulus and strength on the fibre axis were measured at room temperature and at strain rates of 1×10^{-3} and 1×10^{-2} s^{-1}, respectively. The modulus was determined from the slope of the stress–strain curve at low strain ($< 0.1\%$). Dynamic loss modulus was measured by an Orientec viscoelastometer Rheovibron DDV-II-EP operated at a frequency of 3.5 Hz and at a heating rate of 1°C min^{-1}.

RESULTS AND DISCUSSION

The drawability and the tensile properties of drawn films of i-PP and other polymers have been shown to be significantly affected by several factors, including initial morphology, sample molecular weight, stereoregularity and draw technique[15, 22]. Thus, highly syndiotactic PP samples having different initial morphologies (SGC, MSC and MQ) were prepared and drawn by three techniques to study the drawing behaviour, and the resultant tensile and morphological properties. These properties of s-PP were compared to those of i-PP having comparable M_w, M_w distribution and stereoregularity.

Tensile drawing

SGC mats of s-PP were brittle and draw was not

attainable by a straight tensile drawing. Although MSC films of s-PP could be elongated to a strain of ~ 550% at room temperature, the drawn films markedly shrank on removal from the cramps and the resultant *DR* was 3–4. Further, the cold-drawn films had a poor chain orientation and crystallinity. At elevated temperatures of 120–145°C, the MSC films fractured at a lower strain ≤ 100%. However, MQ films of s-PP could be effectively tensile-drawn at elevated temperatures, exhibiting no significant shrinkage after drawing.

Figure 1 shows the maximum achievable *DR* (DR_{max}) as a function of temperature (T_d) for tensile drawing of s-PP MQ films. Drawing was made at a constant cross-head speed giving an initial strain rate ($\dot{\gamma}$) of 2 min^{-1}. The maximum achieved *EDR*s for solid-state coextrusion of s-PP were also included. Among the morphologies of s-PP examined, the MQ film showed a highest achievable *DR* of 8–10 by tensile drawing at the optimum T_d of 145°C and $\dot{\gamma}$ of 2 min^{-1}.

The nominal draw stress vs. strain curves for drawing of the MQ films of s-PP and i-PP are compared in *Figure 2*. These curves were recorded at room temperature and 145°C at constant cross-head speeds giving an initial $\dot{\gamma}$ of 2 min^{-1}. At room temperature, both PPs exhibited yielding at a strain of 10–20%, followed by neck deformation at higher strains. After the neck region, the draw stress increased rapidly with strain for both PPs, and the test specimens fractured at a strain of ~500%. The draw stress of s-PP was significantly lower than that of i-PP over the whole range of strain. At an elevated temperature of 145°C, the i-PP MQ sample showed clear yielding at a low strain, followed by neck deformation. In contrast, the s-PP MQ sample exhibited no necking and was deformed uniformly, probably due to the low crystallinity (29%) compared to the i-PP MQ sample (57%). Further, no significant strain hardening occurred on drawing of the i-PP at 145°C, i.e. the nominal stress increased slowly to a strain of 17 and then decreased slowly at higher strains. Thus, i-PP MQ films could be drawn to a DR_{max} ~ 30 under the condition that was optimum for the s-PP MQ films (T_d145°C, $\dot{\gamma}$ = 2 min^{-1}). The i-PP MSC films could also be drawn to a *DR* ~ 30 under comparable conditions. Thus, for tensile drawing, s-PP exhibited significantly poorer drawability compared to i-PP, independent of the initial morphologies.

Extrusion drawing

The solid-state coextrusion technique developed by Porter *et al.*[18] was also used for drawing of s-PP samples. This technique has been shown to be often applicable for drawing of brittle materials, which could not be elongated by a straight tensile drawing. The maximum achieved extrusion draw ratio (EDR_{max}) for SGC, MSC and MQ of s-PP are shown in *Figure 1* as a function of extrusion temperature (T_e). The SGC and MSC samples could be drawn to an *EDR* ~ 6 at the optimum T_e of 110°C. At a given T_e, s-PP-1 and s-PP-2 showed different drawability. However, the maximum achieved *EDR* for these PPs, having slightly different molecular characteristics, were comparable, as seen in *Figure 1*. The MQ film with a lower crystallinity exhibited a significant elastic shrinkage after extrusion drawing, and the resultant EDR_{max} was 4.7 at the optimum T_e of 125°C. Such shrinkage was lower for the sample with higher crystallinity, and higher EDR_{max} was achieved for the samples with higher initial crystallinity (SGC > MSC > MQ). For tensile drawing of the MQ film at elevated temperatures, such shrinkage was significantly suppressed, and a higher *DR* was attained than for solid-state extrusion.

Second-stage tensile drawing was also attempted for the extrudates. However, no higher *DR* was attainable for s-PP, independent of the initial morphology and *EDR*. The i-PP MSC film could be extrusion drawn to *EDR* ≤ 7.5 at T_e of 110°C and ≤ 11.5 at 130°C. These results also show that s-PP exhibits significantly poorer ductility compared to i-PP, independent of the initial morphologies and techniques used in this work.

Morphological change during drawing

A transmission electron micrograph of solution-grown

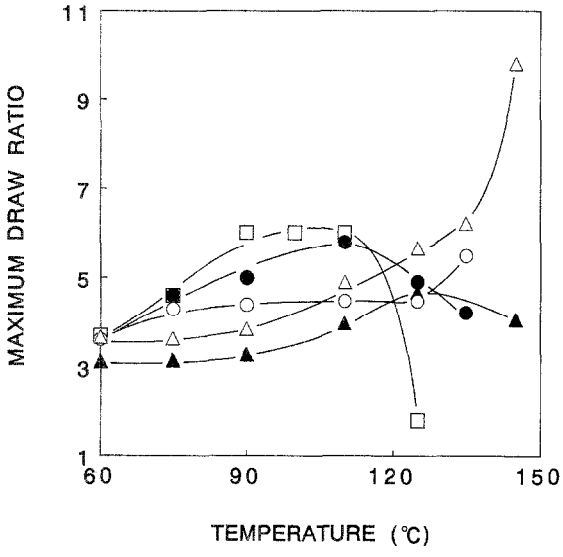

Figure 1 Maximum achieved draw ratio for s-PP morphologies vs. temperature. Extrusion drawing of SGC mat (□) and MSC (●) of s-PP-2, and MQ (▲) and MSC (○) of s-PP-1, and tensile drawing of MQ of s-PP-1 (△)

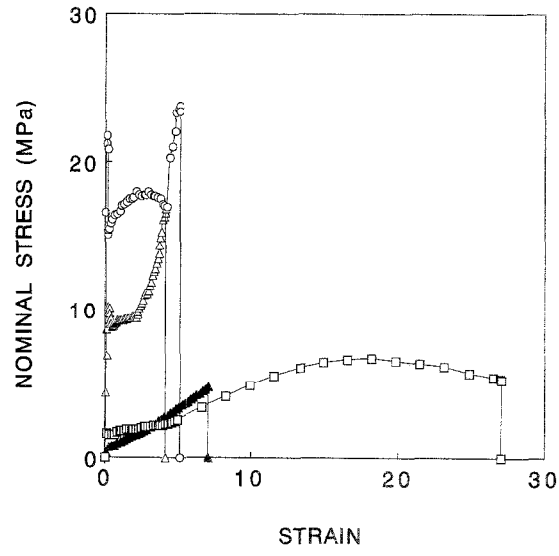

Figure 2 Nominal stress–strain curves for drawing of s-PP MQ at 27°C (△) and 145°C (▲), and i-PP MQ at 27°C (○) and 145°C (□). The curves were recorded at a constant cross-head speed giving an initial strain rate of 2 min^{-1}

crystals of s-PP, precipitated from 0.2 wt% solution in xylene at 45°C, is shown in *Figure 3*. The micrograph shows elongated lamellar crystals several micrometres long and $\sim 0.1\,\mu$m wide. Although we failed to obtain electron diffraction patterns of a single lamella, Lotz *et al.*[3] have shown that the crystallographic *b* axis is parallel to the long axis of the lamella, based on the electron diffraction pattern.

Figure 4 shows sets of WAXD and SAXS patterns obtained with the incident beam both perpendicular (⊥, through view) and parallel (||, edge view) to the wide surface of an SGC mat of s-PP and its *EDR* series prepared at 110°C. All the reflections of the WAXD patterns in *Figure 4* were assigned to those from the most stable form I crystal, which has a $-T_2G_2-$ chain conformation (4_1 helix)[3,4,23]. Two orthorhombic unit cells differing in symmetry have been proposed for form I. Natta *et al.*[2] report that the space group of this form I is $C222_1$ ($a = 14.5$, $b = 5.6$, $c = 7.4$ Å), whereas Lovinger *et al.*[3,4] have proposed *Ibca* with a higher symmetry and having a doubled *b* dimension of Natta's cell ($a = 14.5$, $b = 11.2$, $c = 7.4$ Å). The subscripts N and L of the reflections in *Figure 4* represent the crystal form I proposed by Natta *et al.*[2] and Lovinger *et al.*[3,4], respectively. The reflections with no subscript could be indexed by assuming either of the unit cells. Based on the reflections in *Figure 4A*, the crystal modification of the SGC mat was identified with the L type of form I. Further, the edge view of the WAXD pattern of the mat showed that the intensity maxima of the (2 0 0) and $(0\,2\,0)_L$ reflections were on the meridian, indicating that the crystalline chains were oriented perpendicular to the mat surface. The SAXS pattern of the mat showed that lamellae with long period of 70 Å oriented parallel to the mat surface. These results revealed that the molecular chains were oriented perpendicular to, and the lamellae were aligned parallel to, the surface of the SGC mat.

The SAXS patterns of extrudates exhibited new long-period scattering on the meridian, in addition to the initial equatorial ones. The intensity of the meridional scatterings increased with *EDR* at the expense of the equatorial one. The meridional and equatorial scattering maxima corresponded to the long periods of 120–140 and 70–80 Å, respectively, depending on the sample

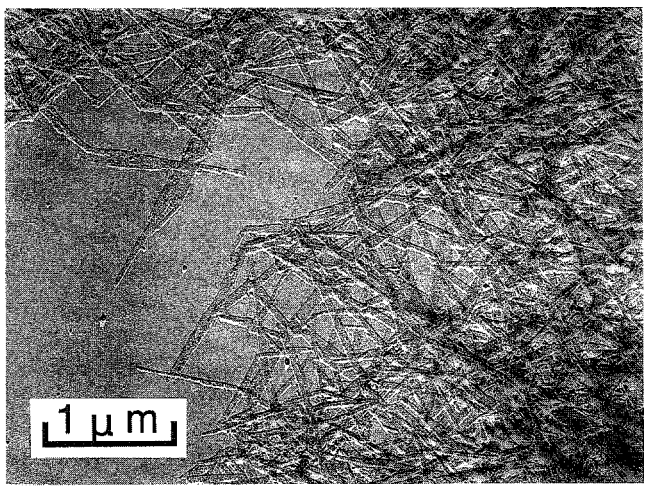

Figure 3 Transmission electron micrograph of solution-grown crystals of s-PP, isothermally precipitated from 0.2 wt% xylene solution at 45°C

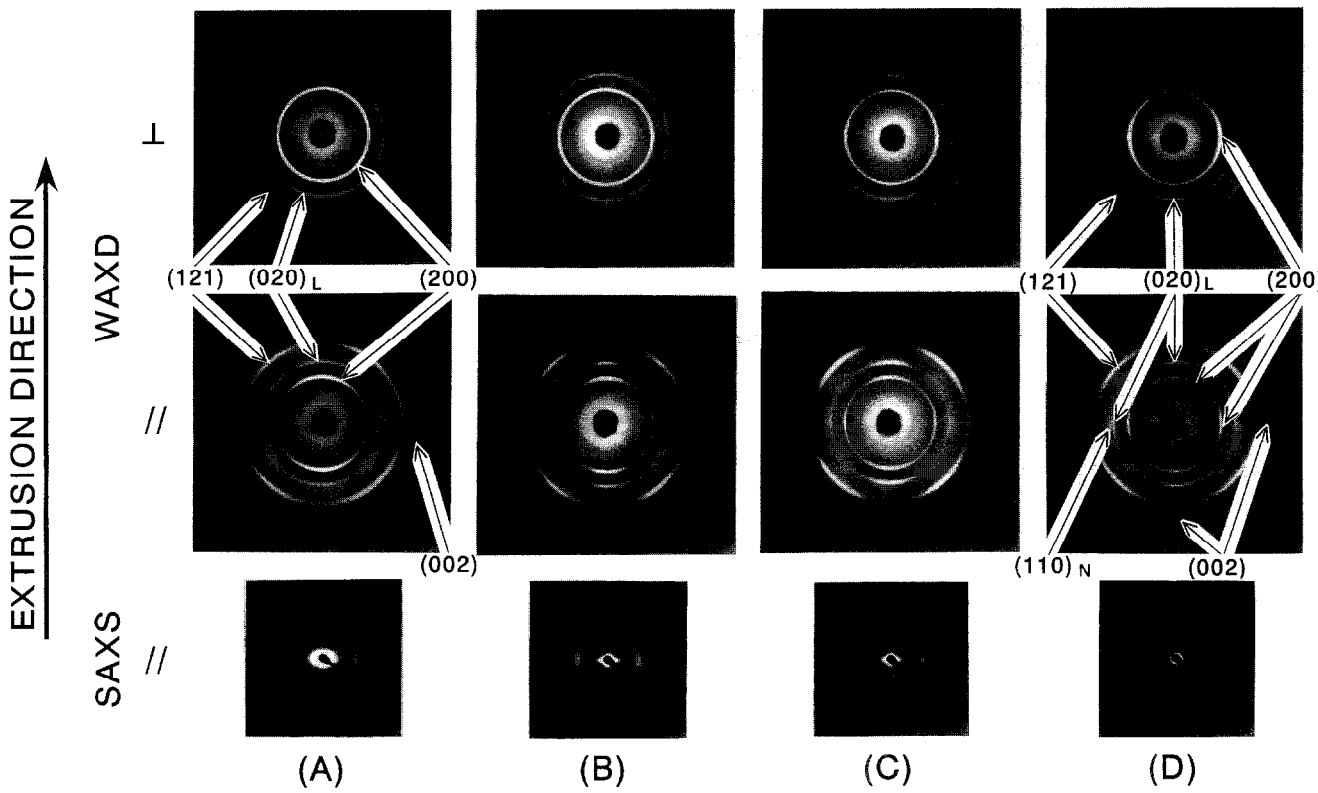

Figure 4 WAXD and SAXS patterns for an *EDR* series of s-PP SGC mats prepared at $T_c = 110$°C: (A) mat, (B) *EDR* = 1.8, (C) *EDR* = 2.9 and (D) *EDR* = 5.5. The subscripts N and L represent the crystal form I having different space groups and unit cells proposed by Natta *et al.*[2] and Lovinger *et al.*[3,4], respectively. The reflections with no subscript could be indexed by assuming either of the unit cells

EDR. This indicates that part of the lamellae, initially oriented parallel to the mat surface, were transformed into a fibrous structure and rearranged to thicker crystals within the microfibrils formed during extrusion drawing. Thus, the extrudates contained two kinds of crystals having different thickness and chain orientation. This morphological feature is consistent with the four-point SAXS patterns and the appearance of the (0 0 2) reflection on both the meridian and equator for the WAXD patterns of the extrusion-drawn films.

For extrusion at a constant temperature of 110°C, the meridional long period of the deformed crystals decreased with increasing *EDR*, i.e. 140 Å at $EDR = 1.8$ and 120 Å at $EDR = 5.5$. Peterlin *et al.*[24] have shown that, on drawing of lamellar crystals, they transformed into the fibrous structure. The long period of the crystal blocks, reorganized into microfibrils, was determined by the draw temperature, and independent of the initial lamellar thickness. Further, they found that the long period increased with draw temperature in the same way as it increased with crystallization temperature. For solid-state extrusion at $T_e = 110$°C, a higher pressure was applied to achieve a higher *EDR*, i.e. 100 atm for $EDR = 1.8$ and 250 atm for $EDR = 5.5$. Thus, the observed decrease of the new long period with increasing *EDR* is attributed to the structural reorganization that occurred at a higher supercooling, as a result of the increased melting temperature due to the application of a higher pressure for extrusion at 110°C.

As mentioned above, some of the initial lamellae, oriented parallel to the mat surface, survived even for an extrudate of $EDR = 5.5$. The long period of such remaining lamellae was slightly larger than that of the initial lamellae, owing to the annealing during and/or after extrusion at 110°C (70 Å for the mats and 80 Å for the extrudate).

The $(1\,1\,0)_N$ reflection, which was absent for the SGC mat, was clearly observed on the equator for the extrudates with higher *EDR*, indicating that they were attributed to the deformed crystals. Thus, a part of the initially L-type crystals were transformed to the N type by the deformation during extrusion. The WAXD through view of the extrudates showed that the (2 0 0) reflection intensity gradually concentrated on the equator and the $(0\,2\,0)_L$ on the meridian with increasing *EDR*. These changes in WAXD, consistent with the SAXS patterns in *Figure 4*, show that the *b* axis, and hence the long axis of the surviving lamellae, was preferentially oriented along the draw direction and the *a* axis perpendicular to it, owing to the slippage of lamellae during extrusion drawing.

Figure 5 shows sets of WAXD and SAXS patterns obtained with the edge and through views for an *EDR* series of s-PP MSC, prepared at 110°C. The SAXS pattern of the initial MSC film showed that the lamellae were partially oriented perpendicular to the film surface. The crystal structure of this sample was also found to be the type L of the form I, since all the WAXD reflections on *Figure 5A* were indexed by assuming this modification. Both the through and edge views of the extrudates show that the intensity of the (2 0 0) and $(0\,2\,0)_L$ reflections rapidly concentrated on the equator, with increasing *EDR*. These patterns show a significantly rapid chain orientation, compared to that observed for extrusion drawing of the SGC mat. The extrudates with a higher *EDR* showed the $(1\,1\,0)_N$ and $(2\,0\,1)_N$ reflections, which were absent for the initial film. The SAXS pattern of an $EDR = 1.9$ extrudate (*Figure 5B*) showed four slightly off-equatorial scatterings, in addition to the strong original ones on the meridian, indicating that a part of the initial lamellae were inclined at an angle to the perpendicular direction to the draw axis. On further extrusion drawing to $EDR > 3.3$, the SAXS patterns revealed a predominantly fibrous morphology. The long period decreased from the initial 115 Å for the undrawn sample to 130 Å at an *EDR* of 5.2. Such a decrease in the meridional long period is also related to the structural transformation that occurred at an increased supercooling[24], which was caused by the pressure applied for extrusion drawing, as discussed above for drawing of the SGC mat.

The MQ sample of s-PP also consisted of the form I of the L type. On tensile drawing of this sample at 145°C, the weak (1 1 0), (0 2 1) and (1 1 1) reflections from the unstable form II crystals (planar zigzag chain conformation, and an orthorhombic cell with $a = 5.22$, $b = 11.17$, $c = 5.06$ Å)[6] appeared, although most of the strong reflections were indexed by the L type of form I crystal. The chain orientation of the tensile-drawn MQ films was as high as that achieved for the extrusion-drawn MSC films (*Figure 5D*).

The total chain orientation, including both the crystalline and amorphous regions, was evaluated by the birefringence (Δn). *Figure 6* shows Δn as a function of *DR* for extrusion-drawn SGC mats and MSC of s-PP, and for tensile-drawn MQ of s-PP. The birefringence Δn increased rapidly with *DR* for each of the samples. However, the increase of Δn for drawing of SGC mats was significantly lower than for the MSC and MQ, owing to the characteristic orientation of the lamellae, resulting in poor chain orientation along the draw direction, as discussed above based on the WAXD and SAXS patterns (*Figure 4*).

Figure 7 shows the crystallinity as a function of *DR* for extrusion drawing of s-PP SGC and MSC at $T_e = 110$°C, and for tensile drawing of s-PP MQ at $T_d = 145$°C. The crystallinity increased rapidly with *DR* for drawing of MSC and MQ. However, it stayed almost constant $\sim 60\%$ for extrusion drawing of the SGC mat, which had the highest crystallinity among the morphologies examined in this work. Thus, the maximum crystallinity achieved by drawing was only $\sim 55\%$, compared to $\sim 70\%$ for the drawn i-PP. Even the well annealed MSC samples of the s-PPs used in this work showed a crystallinity of $\sim 50\%$, as reported in a previous paper[12].

Tensile properties

Figure 8 shows the tensile modulus as a function of *DR* for extrusion and tensile drawing of s-PP and i-PP having different initial morphologies. Extrusion drawing of SGC mats and MSC of s-PP was made at an optimum temperature of 110°C and MSC of i-PP at 130°C. The tensile drawing of MQ films of s-PP and i-PP was carried out at 145°C, which was optimum for the former sample. For drawing of s-PP morphologies, the maximum achieved tensile modulus was significantly higher for the SGC mat than for melt-crystallized samples (3 vs. 1.5–1.8 GPa). The higher modules achieved for the SGC mat is ascribed primarily to the higher crystallinity of

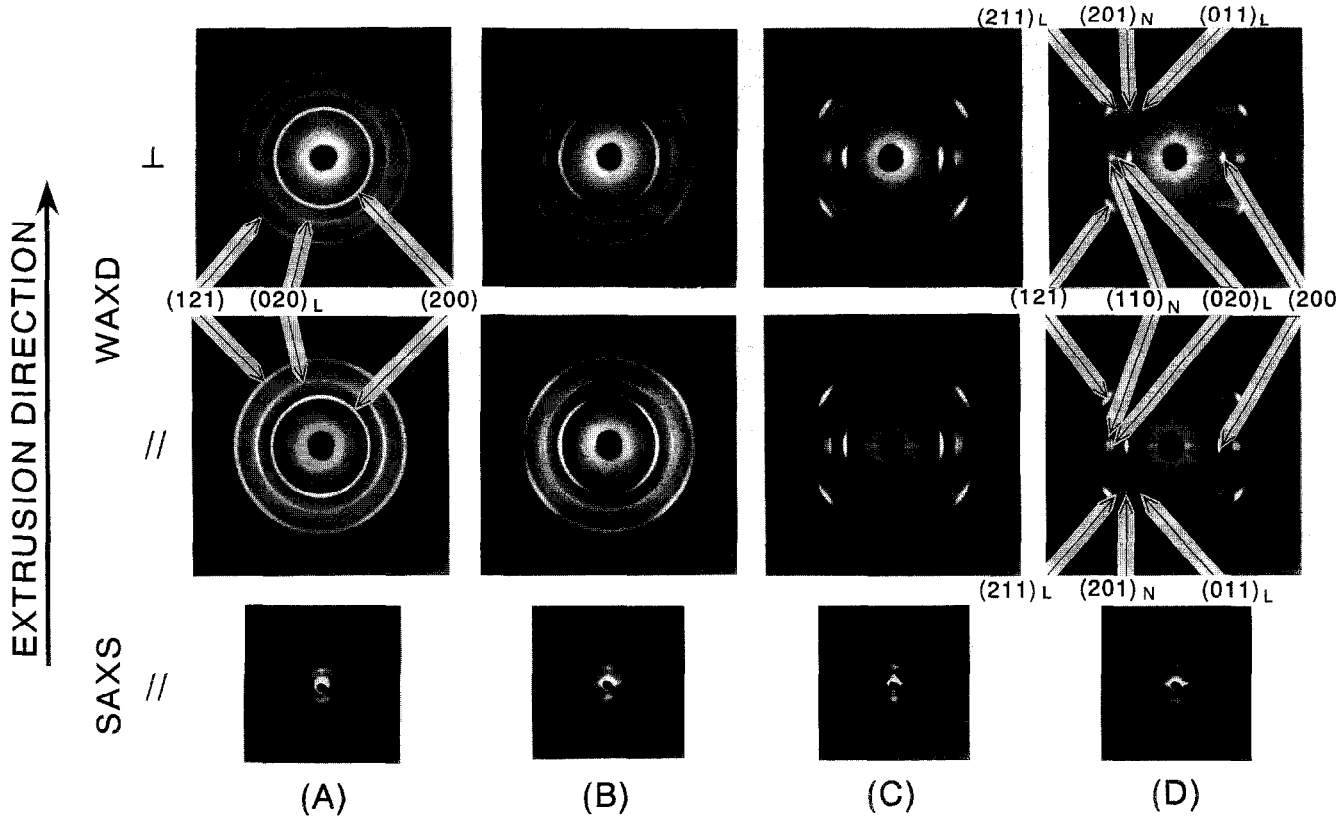

Figure 5 WAXD and SAXS patterns for an *EDR* series of s-PP MSC prepared at T_e = 100°C: (A) initial film, (B) *EDR* = 1.9, (C) *EDR* = 3.3 and (D) *EDR* = 5.2. The subscripts N and L have the same meaning as in *Figure 4*

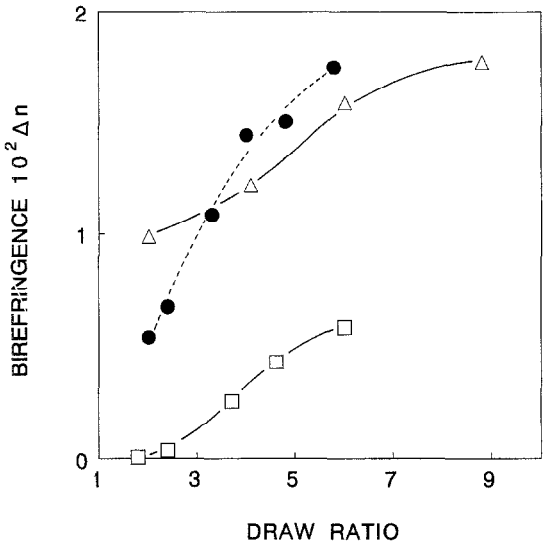

Figure 6 Birefringence vs. *DR* for extrusion drawing of s-PP SGC mats (□) and MSC (●), and for tensile drawing of s-PP MQ (△)

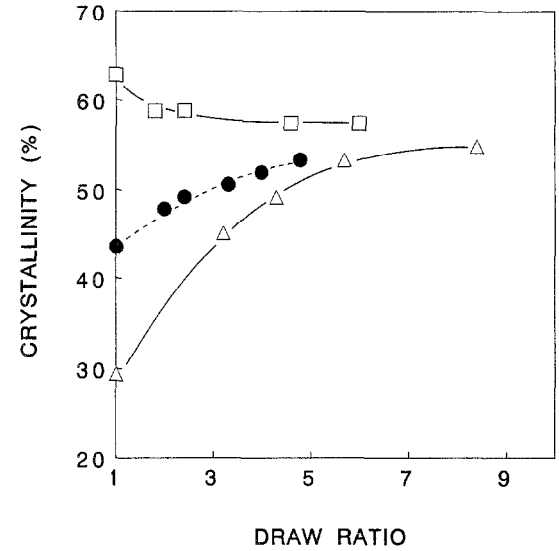

Figure 7 Crystallinity vs. *DR* for extrusion drawing of s-PP SGC mats (□) and MSC (●), and for tensile drawing of s-PP MQ (△)

drawn products than those of drawn MSC and MQ (*Figure 7*), since the chain orientation was significantly lower for the former sample. Thus, the maximum tensile modulus for s-PP was 3 GPa, and achieved by solid-state coextrusion of the SGC mat. This modulus value corresponds to 38% of the X-ray crystal modulus along the chain axis of the crystal form I, recently reported by Nishino and Nakamae (8 GPa)[14]. They also reported that the unstable form II crystal, taking a planar zigzag chain conformation, has a higher crystal modulus of 66 GPa. Thus, oriented films consisting of the form II were also prepared by tensile drawing of the MQ sample in ice–water. The tensile moduli of the cold-drawn samples were low and 0.6 GPa at the maximum achieved *DR* of 3.2, since these samples had poor crystallinity and chain orientation.

Figure 9 shows the tensile strength as a function of *DR* for extrusion drawing of the SGC mat and MSC of s-PP (T_e = 110°C) and the MSC of i-PP (T_e = 130°C), and for tensile drawing of the MQ samples of s-PP and i-PP (T_d = 145°C). The strength increased rapidly with *DR*, except for the SGC mat. At a given *DR*, the strengths of

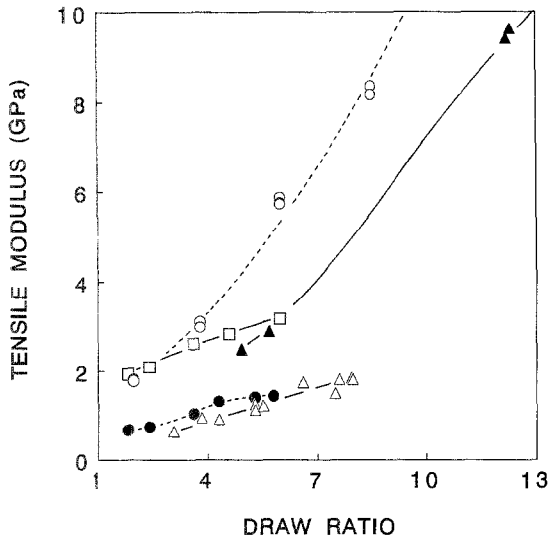

Figure 8 Tensile modulus. vs. *DR* for extrusion drawing of s-PP mats (□), s-PP MSC (●) and i-PP MSC (○), and for tensile drawing of s-PP MQ (△) and i-PP MQ (▲)

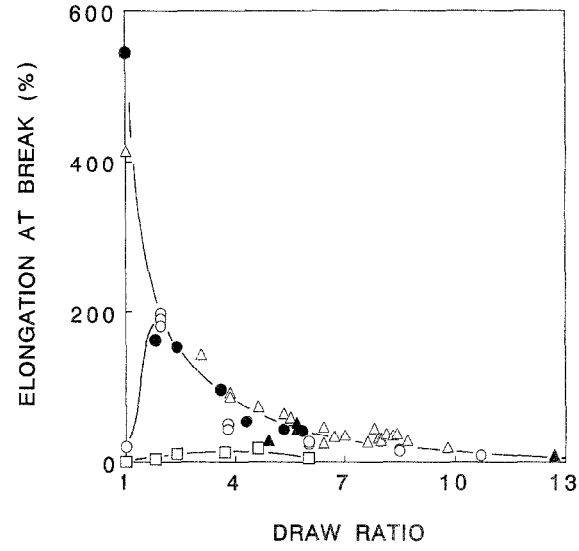

Figure 10 Elongation at break vs. *DR* for extrusion drawing of s-PP SGC mats (□), s-PP MSC (●) and i-PP MSC (○), and for tensile drawing of s-PP MQ (△) and i-PP MQ (▲)

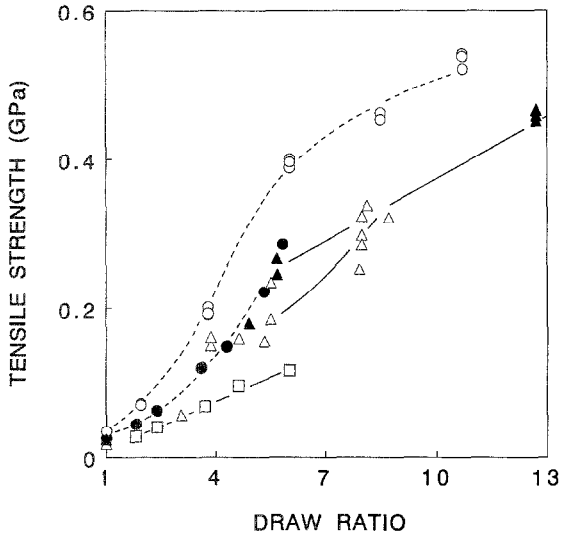

Figure 9 Tensile strength vs. *DR* for extrusion drawing of s-PP SGC mats (□), s-PP MSC (●) and i-PP MSC (○), and for tensile drawing of s-PP MQ (△) and i-PP MQ (▲)

drawn s-PP-1 and s-PP-2 were also comparable. The maximum strength achieved for s-PP samples was 0.30 GPa for extrusion of the MSC and 0.33 GPa for tensile drawing of the MQ at DR_{max} of 5.8 and 8, respectively. These values are comparable to those of drawn i-PP MQ at the corresponding *DR*, yet slightly lower than those of the extrusion-drawn i-PP MSC. Thus, at the same *DR*, the tensile strength of s-PP and i-PP were not so significantly different as was found in the modulus vs. *DR* (*Figure 8*). The strength of drawn SGC mat of s-PP was significantly lower than those drawn from the melt-crystallized morphologies. This trend is the reverse of that found in the modulus vs. *DR*; the modulus was markedly higher for drawn SGC mats (*Figure 8*). The low strength of drawn SGC mats is related to the lower strain at break, as will be discussed later (*Figure 10*). This suggests that the morphological continuity within the drawn samples has not yet been well developed, since lamellar slippage suppressed chain extension and orientation. As a result of the comparable tensile strength for the s-PP and i-PP at a given *DR*, and the markedly lower drawability for the former (*DR* of 10 vs. 30), the maximum achievable tensile strength was significantly lower for the s-PP than for the i-PP (0.33 vs. 0.60 GPa). The poor ductility of s-PP compared to i-PP will be discussed later.

Figure 10 shows the elongation at break as a function of *DR*, measured at room temperature, for the extrusion-drawn SGC mats and MSC of s-PP (T_e = 110°C) and MSC of i-PP (T_e = 130°C), and for the tensile-drawn MQ films of s-PP and i-PP (T_d = 145°C). The SGC mat of s-PP was brittle and the elongation at break was not significantly improved on extrusion drawing. The elongation of undrawn, melt-crystallized samples was strongly affected by the crystallinity. The highly crystalline MSC of i-PP fractured at a low strain of ~ 20%, whereas the MQ of i-PP and the MSC and MQ of s-PP with lower crystallinity showed a larger elongation at break of 400–550%. On extrusion of the initially brittle MSC of i-PP at a low *EDR* of 2.0, the elongation increased significantly from the initial ~ 20% to ~ 190%, followed by a gradual decrease at higher *EDR*. In contrast, the elongation of the highly ductile melt-crystallized i-PP (MQ) and s-PP (MSC and MQ) decreased rapidly with increasing *EDR*, as has often been observed for other polymers[25].

As discussed above, s-PP showed a low drawability compared to i-PP having a comparable M_w, M_w distribution and stereoregularity. Takayanagi[26, 27] proposed that the most effective and highest drawing was achieved slightly above the crystalline relaxation temperature, where molecular motions in the crystalline phase were activated, resulting in the softening of the crystals. Subsequently, Aharoni *et al.*[28] have also shown that the presence of a crystalline relaxation could be a sound criterion for the drawability of polymers; the polymers exhibiting a reversible crystal–crystal transition were highly drawable above its temperature, whereas those showing no such transition exhibited poor ductility. *Figure 11* shows the temperature dependence of the dynamic loss modulus (E'') for the MSC

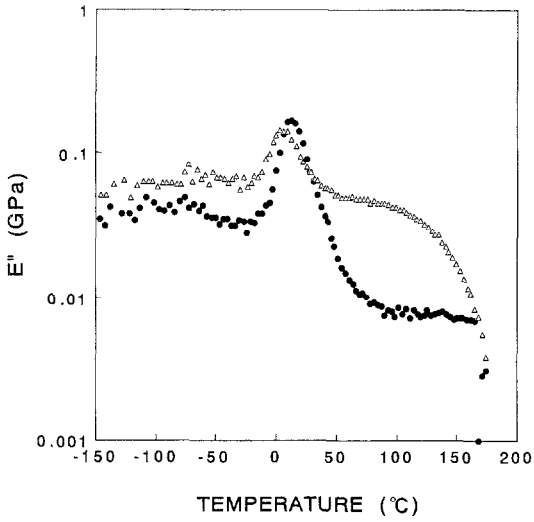

Figure 11 Temperature dependence of the dynamic loss modulus for s-PP MSC (●) and i-PP MSC (△)

films of s-PP and i-PP. Measurements were made at a frequency of 3.5 Hz and at a heating rate of 1°C min^{-1}. The i-PP exhibited three relaxations at ~ -70, 0 and 100°C. The γ relaxation at ~ -70°C is attributed to the motion of short segments[29, 30]. The β peak at ~ 0°C corresponds to the glass transition of i-PP. The α relaxation observed at ~ 100°C has been ascribed to the motion of the chains in the crystalline phase. It has been shown that the drawability of i-PP was remarkably improved above the crystalline dispersion temperature of ~ 100°C[22,28,31]. For s-PP, the γ and β relaxations appeared at ~ -70 and 10°C, respectively. However, no crystalline relaxation was observed for this polymer. Thus, the absence of the crystalline relaxation in the form I crystal of s-PP is probably the primary reason for the poor ductility of s-PP, compared to the high drawability of i-PP, which exhibited a clear crystal relaxation.

CONCLUSIONS

Highly syndiotactic PP exhibited a significantly poorer drawability compared to the i-PP having comparable M_w ($\sim 2 \times 10^5$), M_w/M_n (~ 2.5) and stereoregularity (^{13}C n.m.r. pentad fraction of ~ 0.935), independent of the initial morphologies examined in this work. The poor ductility of the s-PP was ascribed to the absence of a crystalline relaxation, which was clearly observed for i-PP exhibiting a high drawability. The tensile properties of drawn s-PP increased with *DR*. However, at the same *DR*, the modulus was significant and the strength was slightly lower for s-PP than for i-PP. Furthermore, both the maximum achievable tensile modulus and strength for s-PP were remarkably lower than for i-PP, since the latter had a high crystal modulus, crystallinity and drawability compared to the former. The maximum tensile modulus and strength of s-PP achieved in this work were 3.0 and 0.33 GPa, respectively. Drawing of s-PP affected the crystal structure, and both N and L types of the form I unit cells, proposed by Natta *et al.*[2] and Lovinger *et al.*[3, 4], respectively, have been observed depending on the *DR* and drawing conditions. The crystals formed from melt and solution consisted of the L-type unit cell. On drawing, however, a part of these crystals transformed to the N-type unit cell.

REFERENCES

1 Ewen, J. A., Jones, R. L., Razavi, A. and Ferrara, J. D. *J. Am. Chem. Soc.* 1988, **110**, 6255
2 Corradini, P., Natta, G., Ganis, P. and Temussi, P. A. *J. Polym. Sci. (C)* 1967, **16**, 2477
3 Lotz, B., Lovinger, A. J. and Cais, R. E. *Macromolecules* 1988, **21**, 2375
4 Lovinger, A. J., Lotz, B., Davis, D. D. and Padden, F. J., Jr *Macromolecules* 1993, **26**, 3494
5 Natta, G., Peraldo, M. and Allegra, G. *Makromol. Chem.* 1965, **75**, 215
6 Chatani, Y., Maruyama, H., Noguchi, K., Asanuma, T. and Shiomura, T. *J. Polym. Sci. (C)* 1990, **28**, 393
7 Chatani, Y. Maruyama, H., Asanuma, T. and Shiomura, T. *J. Polym. Sci. (B)* 1991, **29**, 1649
8 Boor, J., Jr and Youngman, E. A. *J. Polym. Sci. (A-1)* 1966, **4**, 1861
9 Miller, R. L. and Seeley, E. G. *J. Polym. Sci., Polym. Phys. Edn.* 1982, **20**, 2297
10 Balbontin, G., Dainelli, D., Galimberti, M. and Paganetto, G. *Makromol. Chem.* 1992, **193**, 693
11 Rodriguez-Arnold, J., Zhang, A., Cheng, S. Z. D., Lovinger, A. J., Hsieh, E. T., Chu, P., Johnson, T. W., Honnell, K. G., Geerts, R. G., Palackal, S. J., Hawley, G. R. and Welch, M. B. *Polymer* 1994, **35**, 1884
12 Uehara, H., Yamazaki, Y., Otake, C. and Kanamoto, T. *Koubunshi Ronbunshuu* 1994, **51**, 597
13 Asanuma, T. and Shiomura, T. *Koubunshi Kakou* 1992, **41**, 28
14 Nakamae, K., Nishino, T., Kuroki, T., Goto, Y. and Kuroda, S. *Sen-i Gakkai Prepr. (Japan)* 1992, No. F, 43
15 Kanamoto, T. and Porter R. S. in 'Integration of Fundamental Polymer Science and Technology' (Eds P. J. Lemstra and L. A. Kleintjens), Vol. 3, Elsevier Applied Science, London 1989, p. 168
16 Sakurada, I., Ito, T. and Nakamae, K. *J. Polym. Sci. (C)* 1966, **15**, 75
17 Sakurada, I. and Kaji, K. *J. Polym. Sci. (C)* 1970, **31**, 57
18 Griswold, P. D., Zachariades, A. E. and Porter, R. S. *Polym. Eng. Sci.* 1978, **18**, 861
19 Kanamoto, T., Tsuruta, A., Tanaka, K., Takeda, M. and Porter, R. S. *Polym. J.* 1983, **15**, 327
20 Danusso, F., Moraglio, G., Ghiglia, W., Motta, L. and Talamini, G. *Chem. Ind. (Milan)* 1959, **41**, 748
21 Natta, G. and Pergoraro, M. *Atti. Acc. Nazl. Lincei, Rend., Classe Sci. Fis., Mat. Nat.* 1963, **34**, 110
22 Kanamoto, T., Tsuruta, A., Tanaka, K. and Takeda, M. *Polym. J.* 1984, **16**, 75
23 Natta, G., Corradini, P. and Ganis, P. *Makromol. Chem.* 1960, **39**, 238
24 Corneliussen, R. and Peterlin, A. *Makromol. Chem.* 1967, **105**, 193
25 Burke, P. E., Weatherly, G. C. and Woodhams, R. T. in 'High Modulus Polymers, Approaches to Design and Development' (Eds. A. E. Zachariades and R. S. Porter), Marcel Dekker, New York, 1988, p. 459
26 Takayanagi, M. *Koubunshi* 1961, **10**, 289
27 Takayanagi, M. *Kagaku Kougyou* 1966, No. 4, 1
28 Aharoni, S. M. and Sibilia, J. P. *J. Appl. Polym. Sci.* 1979, **23**, 133
29 Sauer, J. A., Wall, R. A., Fuschillo, N. and Woodward, A. E. *J. Appl. Phys.* 1958, **29**, 1385
30 McCrum, N. G. *Makromol. Chem.* 1959, **34**, 50
31 Roy, S. K., Kyu, T. and Manley, R. St J. *Macromolecules* 1988, **21**, 499